# Direct observation of the initial-state distribution of the first electron transferred to slow highly charged ions interacting with a metal surface

Y. Morishita,[1,2,*] R. Hutton,[3] H. A. Torii,[2] K. Komaki,[2] T. Brage,[3] K. Ando,[1] K. Ishii,[4] Y. Kanai,[1] H. Masuda,[5] M. Sekiguchi,[6] F. B. Rosmej,[2,7] and Y. Yamazaki[1,2]

[1]*Atomic Physics Laboratory, RIKEN, Wako, Saitama 351-0198, Japan*

[2]*Institute of Physics, Graduate School of Arts and Sciences, University of Tokyo, Meguro, Tokyo 153-8902, Japan*

[3]*Department of Physics, University of Lund, Box 118, S221 00 Lund, Sweden*

[4]*Department of Engineering Science, Kyoto University, Kyoto 606-8501, Japan*

[5]*Department of Industrial Chemistry, Tokyo Metropolitan University, Hachioji, Tokyo 192-0397, Japan*

[6]*Center for Nuclear Study, University of Tokyo, Riken Campus, Wako, Saitama 351-0198, Japan*

[7]*GSI-Darmstadt, Plasma Physics, Plankstrasse 1, D-64291 Darmstadt, Germany*

(Received 5 December 2003; published 15 July 2004)

The electron transfer process in the interaction of a slow highly charged ion with a metal surface has been studied employing a microcapillary foil as a target. The combination of the target and a visible light spectroscopy allows us to directly evaluate the initial $(n,\ell)$ distributions of the first transferred electrons. It was found that observed lines were primarily attributed to $\Delta n=1$ transitions with relatively high angular momenta ($\ell_i \gtrsim 4$). A cascade analysis revealed that the electron is selectively transferred to $n \approx q_{in}+1$ states with a narrow distribution width of $\delta n \approx 2$ (full width at half maximum). The average initial principal quantum number is consistent with the prediction of the classical over-barrier model.

DOI: 10.1103/PhysRevA.70.012902 PACS number(s): 34.50.Dy, 32.30.Jc

## I. INTRODUCTION

Charge-transfer processes in collisions of a slow highly charged ion (HCI) with a metallic surface have been intensively studied in the last two decades [1–16]. The major motivation has been to study and to establish the scenario of slow HCI surface interactions, which involves primordial electron transfer processes and both formation and decay processes of hollow atom or ion (HA), an atomic system with many electrons in its excited states and many holes in inner shells. The basic scenario established so far is as follows: When a HCI approaches a metal surface, one of the valence electrons is resonantly transferred to a high Rydberg state of the HCI. This is followed by subsequent electron transfers to lower states when the HCI further approaches the surface, i.e., a HA is formed above the surface. Formation processes of the HA have been studied through measurements of energy gains deduced from deflection angles of incident ions [1,2] and total electron yields [3]. The HA so formed then jumps into the target within a time interval of $\lesssim 10^{-13}$ s because it has been accelerated towards the surface due to its own image charge, until it is completely neutralized. The decay processes and structural properties of the HA have been studied through measurements of x rays [4,5] and Auger electrons [6–9]. It is noted that physical quantities extractable from these measurements are those related to processes taking place mainly after the time interval (HA below the surface), and any transition with its lifetime longer than the time interval scarcely takes place above the surface.

In order to overcome the difficulty and to enable the study of the HA above the surface, a technique to combine HCIs and a thin microcapillary foil has been developed [10,11]. The idea is that when HCIs are injected along the capillary tunnels, a fraction of them can transmit through the tunnels and escape in vacuum even after they capture electron(s) from inner walls of the tunnels. In this case, the interaction between the HCIs and the surface is truncated, i.e., (1) HAs in various stages of the evolution near the surface can be studied and (2) any physical processes which take place with a characteristic time longer than $10^{-13}$ s can be studied exclusively by the present method [10–12].

The interaction of a HCI with a metallic microcapillary foil has been theoretically studied [13] employing the classical over-barrier (COB) model [14], which succeeded in reproducing the charge state distribution of the ions downstream of the capillary [11,15]. Recently, an insulator microcapillary target is reported to have an interesting character, i.e., a HCI beam is guided along the capillary axis keeping their initial charge state even when the capillary is tilted with respect to the HCI beam [16].

In the present paper, we report the very beginning of the HA formation process in HCI surface interaction studied by a spectroscopic method in the visible light range. Such a study becomes feasible only when microcapillaries are used as targets, because the time interval for a flat surface is too short to emit photons in the visible light range where typical transition rates are around $10^9$ s$^{-1}$.

The transition energy $\Delta E(\Delta n)$ of an electron in a high Rydberg state with a principal quantum number $n_i$ of a HCI with its core charge $q_{in}$ is approximately given by

$$\Delta E(\Delta n) \approx \frac{-q_{in}^2}{2n_i^2} + \frac{q_{in}^2}{2(n_i-\Delta n)^2} \approx \frac{q_{in}^2 \Delta n}{n_i^3} \approx \frac{\Delta n}{q_{in}}, \qquad (1)$$

where $\Delta n (\ll n_i)$ is the change in the principal quantum number. The last relation was derived using $n_i \approx q_{in}$ [14] (atomic

*Electronic address: morisita@radphys4.c.u-tokyo.ac.jp

 

units are used unless otherwise noted). Equation (1) indicates that the transition energy for $\Delta n=1$ is in the visible light range when $q_{in}$ is around ten.

## II. EXPERIMENT

The experiments were performed with a 14.25 GHz HyperECR ion source at the Center for Nuclear Study, University of Tokyo, and a 14.5 GHz CapriceECR ion source at RIKEN. $Ar^{q_{in}+}$ ions with $6 \leqslant q_{in} \leqslant 10$ were extracted from the ion sources with energies of 2.0 and 0.88 keV/amu. After charge state selection by an analyzing magnet, the ion beam was collimated to ~1 mm in diameter. The ion beam then impinged upon a Ni microcapillary foil of ~700 nm in thickness with a multitude of straight holes of ~100 nm in diameter [17]. A mirror imaging system was prepared to collect photons emitted from transmitted ions with its half conical angle of 2.9°, and to focus them with one to one imaging on an entrance slit of a Czerny-Turner-type spectrometer. After the spectrometer, photons were detected with a back-illuminated charge-coupled device (CCD) having a pixel size of 24 $\mu$m. The target position is variable along the beam direction so that decay curves can be obtained (see Ref. [18] for more details).

The population of each $(n,\ell)$ state, $N_{n,\ell}(t)$, evolves according to the rate equation

$$dN_{n,\ell}(t)/dt = -(1/T_{n,\ell})N_{n,\ell}(t) + f_{n,\ell}(t), \tag{2}$$

where $t$ is the traveling time of the HCI between the exit of the capillary and the object point of the mirror imaging system, $T_{n,\ell}$ is the lifetime of the $(n,\ell)$ state and $f_{n,\ell}(t)$ is cascade feeding to the $(n,\ell)$ state from upper states.

An observed line intensity $I_{n,\ell}^{n',\ell'}$ for the $(n,\ell)-(n',\ell')$ transition (whose transition rate is $A_{n,\ell}^{n',\ell'}$) with this setup is then given by the solution of Eq. (2) by

$$I_{n,\ell}^{n',\ell'} = \int_{t}^{t+\Delta t} A_{n,\ell}^{n',\ell'} N_{n,\ell}(t')dt', \tag{3}$$

$$= T_{n,\ell} A_{n,\ell}^{n',\ell'} N_{n,\ell}(0) e^{-(t/T_{n,\ell})}[1 - e^{-(\Delta t/T_{n,\ell})}] + g_{n,\ell}(t), \tag{4}$$

where $\Delta t$ is the time window of the detection system and $g_{n,\ell}(t)$ shows a contribution from cascade feeding. Equation (4) reduces to $N_{n,\ell}(0)A_{n,\ell}^{n',\ell'}\Delta t$, assuming $T_{n,\ell} \gg t$, $T_{n,\ell} \gg \Delta t$ and $g_{n,\ell}(t)=0$.

## III. RESULTS AND DISCUSSIONS

Figure 1 shows spectra when 2.0 keV/amu $Ar^{q_{in}+}$ ($q_{in}=6-10$) ions are incident on the Ni microcapillary (spectral resolution: $\Delta\lambda \approx 4$ nm). The spectra are corrected against the detection efficiency of the optical system with respect to wavelengths, i.e., the ordinate is proportional to the number of emitted photons. With the help of Eq. (1), major lines were successfully attributed to $\Delta n=1$ transitions of ions which have eventually captured one, two, or three electrons in the capillary, as discussed later.

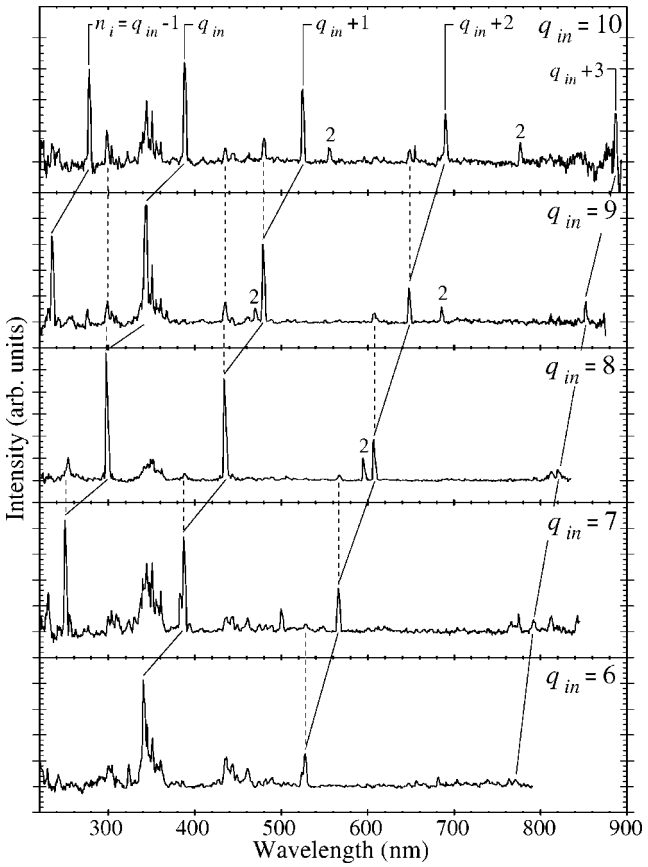


FIG. 1. Wide-range spectra for 2.0keV/amu $Ar^{q_{in}+}$ incident ions. Lines connected by the solid lines are attributed to $\Delta n=1$ transitions of $Ar^{(q_{in}-1)+}$. The solid lines connect transitions with $n_i=q_{in}+s$ among different $q_{in}$ for a fixed $s$. Second-order reflections are marked by 2.

At the top of Fig. 1, $n_i$ involved in each transition is given using the incident charge $q_{in}$ as a parameter. The solid lines connect transitions with $n_i=q_{in}+s$ among different $q_{in}$ for a fixed $s$ ranging from −1 to 3. It is commonly seen that the photon intensities are the maximum for $n_i=q_{in}$ transitions and decreasing monotonously toward $n_i=q_{in}+3$. The present setup is not sensitive to photon energies of $\Delta n=1$ and $n_i \geqslant q_{in}+4$ transitions.

It is also seen that the lines identified above were often observed for higher incident charge states with considerable intensities, which are connected by the broken lines. This shows that multiple electron transfers take place in the capillary, and a part of the transferred electrons quickly fill core hole(s) via either Auger electron or x-ray emissions, still keeping one electron at a high Rydberg state. Actually, the line intensity variations along the broken lines are similar to the charge state distributions of transmitted ions [11,15].

The broad band structures around 350 and 450 nm were observed for all the charge states. A comparison of high-resolution spectra with compiled data [19] in these wavelength ranges revealed that the structures are attributed to transitions of Ni atoms (350 nm) and $Ar^+$ ions (450 nm) [18]. This fact indicates that the inner wall of the capillary is somewhat sputter cleaned continuously during the experiments.

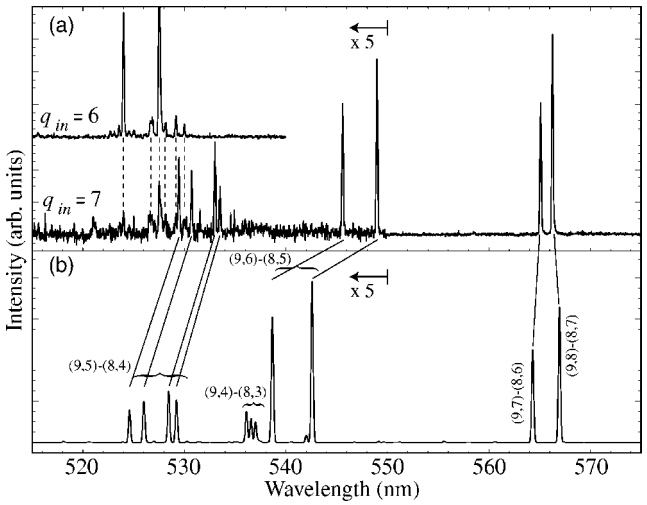


FIG. 2. (a) High-resolution spectra around $n_i=9$ transitions of $Ar^{6+}$ ($q_{in}=7$) and $n_i=8$ transitions of $Ar^{5+}$ ($q_{in}=6$) ions. (b) A spectrum generated using results by MCHF codes. Lines identified are connected by the solid lines.

In order to get quantitative information on the initial-state distribution, the spectra were remeasured with a higher resolution so that transitions belonging to the same $n_i$ and $\Delta n$, but to different angular momentum quantum numbers, $\ell_i$, are distinguished, which is essential to make accurate cascade calculations because the lifetime of each state depends on $\ell_i$.

Figure 2(a) shows an example of high-resolution spectra ($\Delta\lambda \approx 0.15$ nm) around $n_i=9$ transitions of 2.0 keV/amu $Ar^{6+}$ ($q_{in}=7$) ions. Lines belonging to lower charge states than $Ar^{6+}$ ions and to sputtered particles were discriminated by observing spectra for lower charge state ions, an example of which is shown in the upper half of Fig. 2(a) for 2.0 keV/amu $Ar^{5+}$ ($q_{in}=6$) ions (see the spectral lines connected by the dotted lines).

To identify these lines, a theoretical calculation based on the multiconfiguration Hartree-Fock formalism (MCHF) was performed [20]. Due to a small energy difference between the ground ($1s^22s^22p^63s$) and the first excited ($1s^22s^22p^63p$) states of the ionic core (0.64 a.u. [21]), the configuration interaction between the $3sn\ell$ and the $3pn'\ell'$ states becomes very important. In the calculation, $3\ell 3\ell'$, $3sn_1\ell$, $3pn_2\ell$, and $3dn_3\ell$ configurations with $n_1=4-11$, $n_2=4-6$, and $n_3=4-5$ were taken into account. The resultant spectrum is shown in Fig. 2(b), where the line intensities are plotted in proportion to their corresponding transition rates multiplied by their statistical weights and convoluted over the spectrometer resolution. The observed lines were identified by comparing with the predicted line positions and relative intensities.

Lines so identified are connected by the solid lines. It is seen that wavelengths were predicted within ~1% and transitions involving $\ell_i$ as low as 5 were identified. Similar conclusions were obtained also for $n_i=7,8$, and 10 transitions, and Table I(a) summarizes the wavelengths of observed lines and calculated transitions.

High-resolution spectra for 2.0 keV/amu $Ar^{7+}$ ($q_{in}=8$) ions were also studied, which consist only of three strong lines. This is because the ion core is a closed shell ($Ar^{8+}$;

TABLE I. Wavelengths observed in the high-resolution experiment with 2.0 keV/amu (a) $Ar^{7+}$ and (b) $Ar^{8+}$ impinged onto the Ni microcapillary. Precisions of the wavelengths are ~0.1 nm. The second and last columns show calculated wavelengths and are identified $(n_i,\ell_i)$ in the $\Delta n=\Delta\ell=1$ transitions.

(a)

| Observed | MCHF | Transition |
|---|---|---|
| 241.72 | 241.83–.90 | $(7,4)\ ^3G_J-{}^3F_{J-1}$ |
| 247.98 | 250.27 | $(7,4)\ ^1G_4-{}^1F_3$ |
| 250.19 | 248.82–.87 | $(7,6)\ ^{1,3}I_J-{}^{1,3}H_{J-1}$ |
| 255.59 | 254.17–.30 | $(7,5)\ ^3H_J-{}^3G_{J-1}, {}^1H_5-{}^3G_4$ |
| 260.64 | 261.50–.61 | $(7,5)\ ^1H_5-{}^1G_4, {}^3H_5-{}^1G_4$ |
| 383.42 | 380.40–.42 | $(8,6)\ ^3I_{6,5}-{}^3H_{5,4}$ |
| 383.65 | 380.66–.67 | $(8,6)\ ^3I_7-{}^3H_6, {}^3I_6-{}^1H_5$ |
| 387.74 | 387.14–.17 | $(8,7)\ ^{1,3}K_J-{}^{1,3}I_{J-1}$ |
| 393.32 | 392.36–.54 | $(8,5)\ ^1H_5-{}^3G_4, {}^3H_6-{}^3G_5$ |
| 394.78 | 394.33–.42 | $(8,5)\ ^3H_{4,5}-{}^3G_{3,4}$ |
| 395.25 | 395.26 | $(8,5)\ ^1H_5-{}^1G_4$ |
| 397.02 | 397.36 | $(8,5)\ ^3H_5-{}^1G_4$ |
| 529.62 | 524.60 | $(9,5)\ ^3H_4-{}^3G_3$ |
| 530.87 | 526.01 | $(9,5)\ ^3H_5-{}^3G_4$ |
| 533.16 | 528.46 | $(9,5)\ ^3H_6-{}^3G_5$ |
| 533.66 | 529.23 | $(9,5)\ ^1H_5-{}^1G_4$ |
| 545.74 | 538.65–.71 | $(9,6)\ ^3I_{5,6}-{}^3H_{4,5}$ |
| 549.13 | 542.59–.60 | $(9,6)\ ^1I_6-{}^1H_5, {}^3I_7-{}^3H_6$ |
| 565.25 | 564.30–.35 | $(9,7)\ ^{1,3}K_J-{}^{1,3}I_{J-1}$ |
| 566.43 | 566.94–.97 | $(9,8)\ ^{1,3}L_J-{}^{1,3}K_{J-1}$ |
| 789.86 | 788.44–.54 | $(10,7)\ ^{1,3}K_J-{}^{1,3}I_{J-1}$ |
| 791.77 | 792.44 | $(10,8)\ ^{1,3}L_J-{}^{1,3}K_{J-1}$ |
| 792.35 | 792.80 | $(10,9)\ ^{1,3}M_J-{}^{1,3}L_{J-1}$ |

(b)

| Observed | Polarization | Transition |
|---|---|---|
| 294.78 | 294.83 | (8,4) |
| 297.34 | 297.35 | (8,5) |
| 297.63 | 297.61 | (8,6) |
| 297.63 | 297.66 | (8,7) |
| 429.90 | 429.97 | (9,4) |
| 433.65 | 433.70 | (9,5) |
| 434.12 | 434.08 | (9,6) |
| 434.12 | 434.16 | (9,7) |
| 434.12 | 434.18 | (9,8) |
| 600.92 | 601.07 | (10,4) |
| 606.23 | 606.32 | (10,5) |
| 606.93 | 606.85 | (10,6) |
| 606.93 | 606.96 | (10,7) |
| 606.93 | 607.00 | (10,8) |
| 606.93 | 607.01 | (10,9) |

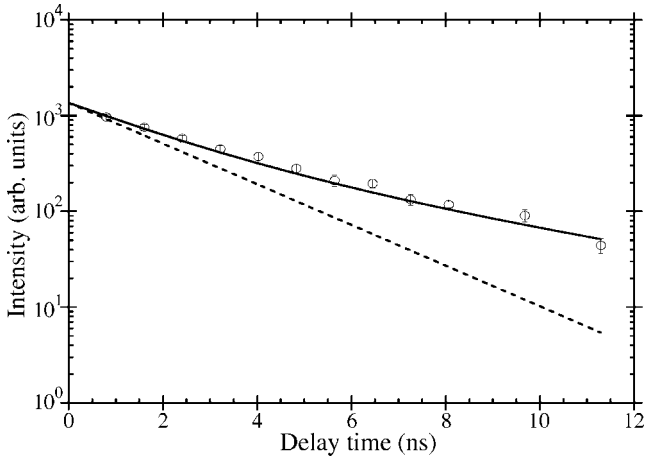


FIG. 3. Decay curve of the $(8,7)-(9,8)$ transition of $Ar^{6+}$. The open circles with error bars are experimental values. The solid line is obtained by the fitting. The dotted line shows the decay curve when only the (9,8) state is populated.

$1s^2 2s^2 2p^6$) and the first excited state ($1s^2 2s^2 2p^5 3s$) is 9.6 a.u. [21] away from the ground state.

The lines were identified by comparing with the prediction of a semiempirical polarization formula [22],

$$E_{n,\ell} = -\mathcal{R}\left(\frac{q_{in}^2}{n^2} + \alpha_d\langle r^{-4}\rangle + \alpha_q\langle r^{-6}\rangle\right), \tag{5}$$

where $\mathcal{R}$ is the Rydberg constant and $\alpha_d$(=0.0313) and $\alpha_q$(=0.0314) are the dipole and quadrupole polarizabilities for $Ar^{8+}$ core [23], and quantities with brackets show expectation values evaluated with hydrogenlike wave functions. Table I(b) summarizes the wavelengths of observed lines and calculated transitions. Initial angular momentum quantum numbers as low as $\ell_i = 4$ were identified within the precisions of 0.02%, however, transitions belonging to $\ell_i \geqslant 6$ are observed just as a single peak in the present spectrometer resolution.

In order to evaluate the initial $(n,\ell)$ distributions, namely, the populations at the very exit of the capillary, decay curves of the transitions in question were measured. The open circles in Fig. 3 show, as an example, the intensity variation of the $(8,7)-(9,8)$ transition of $Ar^{6+}$ ions as a function of delay time. The dotted line shows a predicted intensity variation when only the (9,8) state is populated. The discrepancy results because the (9,8) state is cascade filled from upper states, which have normally longer lifetimes.

To reproduce the decay curve, Eqs. (2) and (4) were solved analytically, taking into account the cascade-filling processes with $n$ as high as $q_{in}+4$, where transition rates were calculated by the MCHF code for the most of the states [24]. The initial populations were, then, determined employing the least-squares method. The solid line in Fig. 3 shows an example of the resultant decay curve for (9,8) state, which reproduces the observation quite satisfyingly.

Figure 4(a) shows the initial $(n,\ell)$ distributions for 2.0 keV/amu $Ar^{7+}$ ions impinging upon the Ni microcapillary. It is seen that the initial $n$ distribution is almost independent of $\ell$, and is peaked at $n=9$. For each $n$ manifold, higher angular momentum states are, in general, preferentially populated, like in the statistical distribution rather than the flat ($\ell$-independent) distribution.

A similar analysis was performed for the 2.0 keV/amu $Ar^{8+}$ incidence, and the resultant distributions are shown in Fig. 4(c) for $\ell = n-1$, $n-4$, $n-5$, and $n-6$ states. Because $\ell_i \geqslant 6$ transitions were not resolved in this case, we assumed a statistical distribution, and the populations for $\ell = n-1$ states are shown as examples.

The average values of $n$ over distributions were 8.4 and 9.5 for $q_{in}=7$ and $q_{in}=8$ ions, respectively, and the full widths at the half maximum of the distributions were $\delta n \approx 2$ for both incident charge states studied.

According to the COB model [14], the first electron transfer takes place at a critical distance, $d_c \approx \sqrt{2q_{in}}/W$, to a state with a principal quantum number,

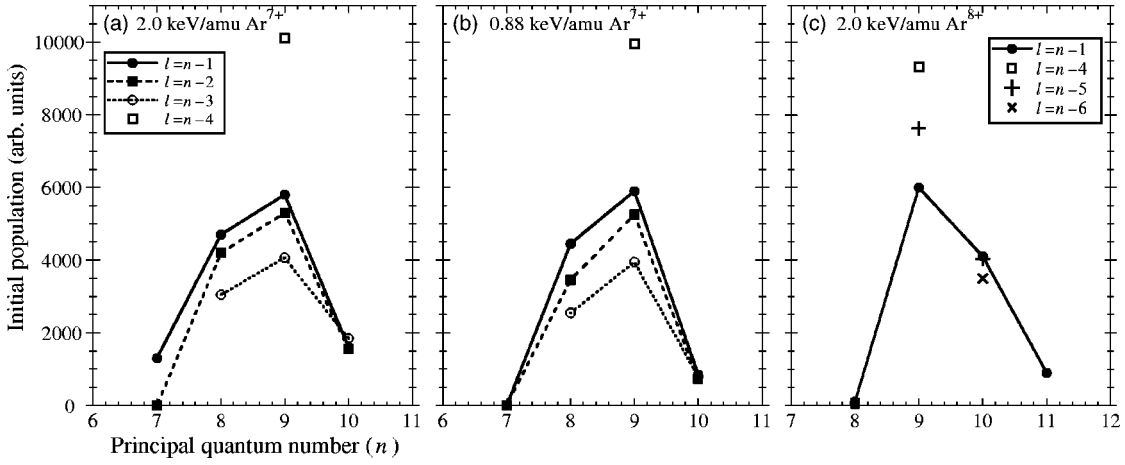


FIG. 4. Distributions of the initial populations for $\ell = n-k$ states for 2.0 keV/amu $Ar^{7+}$ (a) and $Ar^{8+}$ (c) ions. In the case of (c), $\ell$ distributions for $\ell \geqslant 6$ were assumed to be statistical, and populations for $\ell = n-1$ states were plotted (•) because transitions from these states were not resolved. (b) shows the distributions for 0.88 keV/amu $Ar^{7+}$ ions.

$$n_c \approx q_{in}/\sqrt{2W[1+(q_{in}-1/2)/\sqrt{8q_{in}}]} \approx q_{in}+1.3, \quad (6)$$

where $W$ is the work function of the surface. The work function of Ni was chosen to be 0.191 a.u. by averaging published values over different crystalline planes [25]. The last relation in Eq. (6) holds for the charge states used in the present study.

Equation (6) predicts that $n_c$ should be around 8.3 and 9.3 for $q_{in}=7$ and 8, respectively, which agree quite well with the average $n$'s obtained above. Although the $n$ distributions for other charge states were not fully studied, Fig. 1 suggests that $n_c$ predicted by the COB model is also a reliable measure even for $q_{in}=9$ and 10 (note that the most intense lines in Fig. 1 are scaled by $q_{in}$). Although the population of the $(n,\ell)=(9,5)$ state looks irregularly high for $q_{in}=7$ and 8 distributions, it should be noted that accurate estimation is quite difficult for low $\ell$ states because fast decay channels with $\Delta n \gg 1$ become more and more important.

To get an idea on how the angular momentum distribution is determined, the level splittings ($\Delta E_\ell$) among different $\ell$ states with the same $n$ are compared with the Stark splitting induced by the electric field of the image charge, $\Delta E_{ss} \approx 3n(n-1)W^2/16q_{in}$ (here it is assumed that the first electron transfer takes place at the critical distance).

For $q_{in}=7$ and $n=8$, $\Delta E_\ell \approx 0.07$ a.u. is comparable to $\Delta E_{ss} \approx 0.055$ a.u. (except for $s$ and $p$ orbitals, $\Delta E_\ell$ is much smaller than 0.02 a.u.). In other words, different angular momentum states with the same magnetic quantum number are more or less uniformly mixed up, resulting in the statistical distribution. The angular momentum distribution has also been determined for 0.88 keV/amu $Ar^{7+}$ ions, which is shown in Fig. 4(b). The result is the same as that for the 2.0 keV/amu incidence within the experimental uncertainty.

The fact that the angular momentum distribution does not depend on the ion velocity rules out the possibility that the angular momentum of the transferred electron is kinematically determined by $m_e v d_c$ [26], where $m_e$ is the electron mass and $v$ is the ion velocity. Furthermore, it is noted that even the energy difference between $n=q_{in}+1$ and $q_{in}+2$ ($q_{in}=7,8$) states is comparable to the Stark splitting.

Figure 5 shows energies of the two extreme Stark states with $n$ from $q_{in}$ to $q_{in}+4$ as a function of the incident charge $[E^{\pm}(n=q_{in}+s)=-q_{in}^2/2n^2 \pm \Delta E_{ss}]$. The line denoted by $E_{COB}$ shows the energy level at which the first electron transfer is predicted to take place. It is seen that $E_{COB}$ locates just between $E^+(q_{in}+1)$, and $E^-(q_{in}+2)$, locates subtly below $E^-(q_{in}+3)$, and locates far above $E^+(q_{in})$. This means that wave functions formed around the $E_{COB}$ line are those of $n=q_{in}+1$ and $q_{in}+2$ states, which is again consistent with the observed distribution widths of $\delta n \approx 2$.

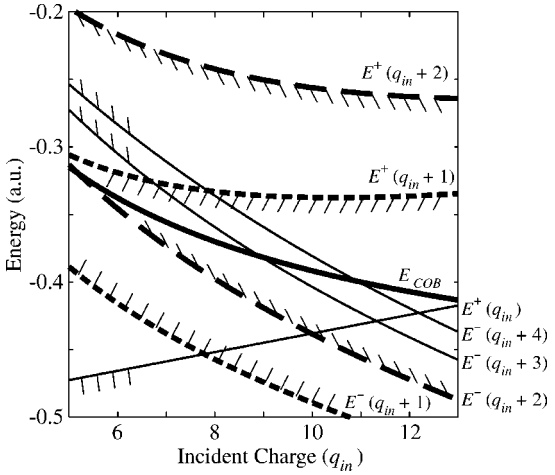


FIG. 5. Energy variations of the two extreme Stark states ($q_{in} \leq n \leq q_{in}+4$) as a function of the incident charge. The line with $E_{COB}$ shows the energy of the first electron transfer predicted by the COB model. It is seen around charge states studied that the $E_{COB}$ line locates just between $E^-(q_{in}+2)$ and $E^+(q_{in}+1)$.

## IV. SUMMARY

We performed high-resolution measurements of visible light emitted from $Ar^{(q_{in}-1)+}$ ions produced in interaction of 2.0 keV/amu $Ar^{q_{in}+}$ ($q_{in}=7,8$) ions with a Ni microcapillary. The line intensities were then evaluated taking into account the cascading from the upper states, which revealed that the electron transfer takes place preferentially to the $n \approx q_{in}+1$ states with the distribution width of $\delta n \approx 2$ (full width at half maximum). The average $n$ value of the populated states was found to be quantitatively consistent with the prediction of the COB model. The $\ell$ distributions are found to be more or less statistical, which are at least qualitatively consistent with the prediction of the Stark mixing model.

[1] H. Winter, Europhys. Lett. **18**, 207 (1992).
[2] F. W. Meyer *et al.*, Nucl. Instrum. Methods Phys. Res. B **98**, 441 (1995).
[3] F. Aumayr *et al.*, Phys. Rev. Lett. **71**, 1943 (1993).
[4] J. P. Briand *et al.*, Phys. Rev. Lett. **65**, 159 (1990).
[5] B. d'Etat *et al.*, Phys. Rev. A **48**, 1098 (1993).
[6] F. W. Meyer *et al.*, Phys. Rev. A **44**, 7214 (1991).
[7] J. Das and R. Morgenstern, Phys. Rev. A **47**, R755 (1993).
[8] S. Schippers *et al.*, Phys. Rev. A **50**, 540 (1994).
[9] M. Grether *et al.*, Phys. Rev. A **52**, 426 (1995).
[10] Y. Yamazaki *et al.*, J. Phys. Soc. Jpn. **65**, 1199 (1996).
[11] S. Ninomiya *et al.*, Phys. Rev. Lett. **78**, 4557 (1997).
[12] Y. Morishita *et al.*, Phys. Scr., T **T80B**, 212 (1999).
[13] K. Tőkési, L. Wirtz, C. Lemell, and J. Burgdörfer, Phys. Rev. A **61**, 020901(R) (2000).
[14] J. Burgdörfer, P. Lerner, and F. W. Meyer, Phys. Rev. A **44**, 5674 (1991).
[15] D. Murakoshi *et al.*, in *XXII ICPEAC Abstracts of Contributed Papers* (Rinton, in NJ, 2001), p. 504.
[16] N. Stolterfoht *et al.*, Phys. Rev. Lett. **88**, 133201 (2002).
[17] H. Masuda and K. Fukuda, Science **268**, 1466 (1995).
[18] Y. Morishita *et al.*, Nucl. Instrum. Methods Phys. Res. B **205**,

758 (2003).
[19] C. Corliss and J. Sugar, J. Phys. Chem. Ref. Data **10**, 1 (1981); V. Vujnović and W. L. Wiese, *ibid.* **21**, 5 (1992).
[20] R. D. Cowan, *The Theory of Atomic Structure and Spectra* (University of California Press, Berkeley, 1981); C. F. Fischer, T. Brage, and P. Jönsson, *Computational Atomic Structure* (Institute of Physics, Bristol, 1997).
[21] R. L. Kelly, J. Phys. Chem. Ref. Data **16**, 1 (1987).
[22] B. Edlén, *Atomic Spectra*, Handbuch Der Physik Vol. XXVII (Springer, Berlin, 1964).
[23] B. Edlén, Phys. Scr. **17**, 565 (1978).
[24] We used experimentally evaluated lifetimes for (9,5) and (8,5) states of $Ar^{6+}$, which suffered from considerable configuration interaction.
[25] B. G. Baker, B. B. Johnson, and G. L. C. Maire, Surf. Sci. **24**, 572 (1971).
[26] J. Burgdörfer, R. Morgenstern, and A. Niehaus, J. Phys. B **19**, L507 (1986).